NANO LETTERS

Letter

pubs.acs.org/NanoLett

Control and Near-Field Detection of Surface Plasmon Interference Patterns

Petr Dvořák,[†,‡] Tomáš Neuman,[†,‡] Lukáš Břínek,[†,‡] Tomáš Šamořil,[†,‡] Radek Kalousek,[†,‡] Petr Dub,[†,‡] Peter Varga,[‡] and Tomáš Šikola*[,†,‡]

[†]Institute of Physical Engineering, Brno University of Technology, Technická 2, Brno 616 69, Czech Republic

[‡]CEITEC BUT, Technická 10, 616 69 Brno, Czech Republic

Supporting Information

ABSTRACT: The tailoring of electromagnetic near-field properties is the central task in the field of nanophotonics. In addition to 2D optics for optical nanocircuits, confined and enhanced electric fields are utilized in detection and sensing, photovoltaics, spatially localized spectroscopy (nanoimaging), as well as in nanolithography and nanomanipulation. For practical purposes, it is necessary to develop easy-to-use methods for controlling the electromagnetic near-field distribution. By imaging optical near-fields using a scanning near-field optical microscope, we demonstrate that surface plasmon polaritons propagating from slits along the metal–dielectric interface form tunable interference patterns. We present a simple way how to control the resulting interference patterns both by variation of the angle between two slits and, for a fixed slit geometry, by a proper combination of laser beam polarization and inhomogeneous far-field illumination of the structure. Thus the modulation period of interference patterns has become adjustable and new variable patterns consisting of stripelike and dotlike motifs have been achieved, respectively.

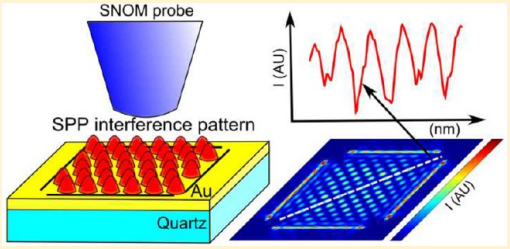

KEYWORDS: *SNOM, near-field detection, plasmon interference, surface plasmon polaritons, near-field optics*

The surface plasmon polaritons (SPPs) are evanescent electromagnetic surface waves coupled to the collective longitudinal oscillations of the free-electron gas in a metal propagating along a metal–dielectric interface.[1−3] Spatial confinement of the electromagnetic field at the interface and smaller wavelength compared to the excitation light, corresponding enhancement of electromagnetic energy density at this interface, and the sensitivity of SPPs to dielectric functions of both material constituents forming the interface make SPPs attractive for many applications.

In addition to general interests in plasmonic-based nanodevices and nanocircuits (2D optics) for optical communication technologies, offering frequencies over 100 THz but still representing a big technology challenge, there are other areas in which plasmonics already finds its applications.[4−6]

It covers photodetection[7] and (bio)sensing with enhanced sensitivity,[8,9] a new generation of photovoltaics,[10] spatially localized spectroscopy (nanoimaging utilizing plasmon enhanced Raman spectroscopy and photoluminescence),[11,12] surface patterning (nanolithography),[13,14] and manipulation of nanoparticles.[15,16]

A series of applications including both the surface patterning and manipulation of nanoparticles take the advantage of the formation of proper interference patterns of SPPs at interfaces. However, there is still a limited number of studies dedicated to exploring the simple ways how to control the SPPs interference patterns. Generally, the papers dealing with the near-field interference patterns have preferentially concentrated on detection and description of the fixed near-field interference patterns and their control has not been the main issue. The first papers already published in this field were particularly aimed at focusing of SPPs into one or two specific focal points with an enhanced electric field.[17−21] Later on, the papers devoted to the formation of interference patterns over a specific flat area, obtained by Young's double slit experiment based on SPPs,[22] and especially the stripelike interference of SPPs launched by two parallel slits, appeared.[23]

Finally, the results on a four-slit experiment were published.[24] In this experiment, a partial control of interference patterns by changing the polarization of the incident light (either stripelike or dotlike interference patterns of SPPs) were achieved. In these papers, except for the change of the polarization light no other measures to control the interference patterns were taken. Contrary to that, in the paper[25] an active spatial control of plasmonic fields was reported. However, this method was conditioned by presence of geometrical structures (e.g., nanoholes) over the whole interference area which limits the number of envisaged applications (e.g., trapping and selective growth). Thus, the control together with mapping of the near-field interference patterns over the flat metallic surfaces is still a challenging issue.

In this paper, we show an easy-to-use way of controlling near-field interference patterns created between the slits on a

Received: February 20, 2013
Revised: April 29, 2013
Published: May 16, 2013

   dx.doi.org/10.1021/nl400644r | *Nano Lett.* 2013, 13, 2558−2563

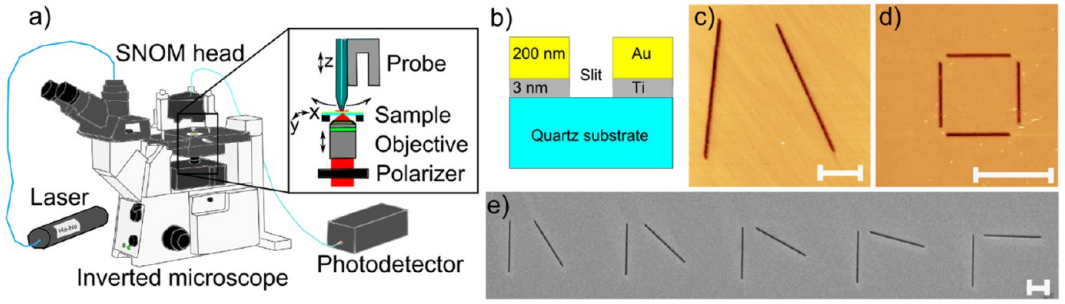

Figure 1. Schematic of SNOM installed on an inverted optical microscope (a). Cross section of the sample (b). Topography of studied SPP interference structures (c), (d). SEM image of interference structures consisting of slit pairs mutually tilted by various angles (e). The scale bars are 5 μm long.

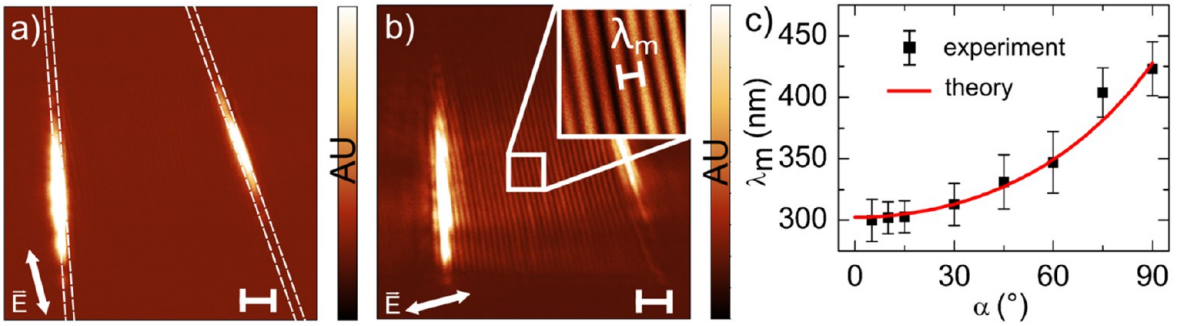

Figure 2. Near-field images of the interference pattern ($|\mathbf{E}|^2$) detected between the slit pair (α = 10°) (a,b). The interference pattern exhibits minimum intensity modulation if illuminated by the laser beam polarized in the direction of the axis of the tilt angle (a) (see the white double arrow), maximum intensity modulation if the incident light is polarized in the perpendicular direction to the axis of the tilt angle (b). The modulation period λ_m is shown in detail. The experimentally measured dependence of the modulation period λ_m on the tilt angle compared with the theoretical prediction calculated according to (eq 1) (c). The scale bars are 2 μm long.

flat Au surface being monitored by SNOM imaging and confronted to those obtained by analytical and numerical models. Such a control has been provided both by variation of the angle between two slits and, for a fixed slit geometry, by a proper combination of laser beam polarization and inhomogeneous far-field illumination of the structure. In this way, the limits in controlling SPP interference patterns can be partially overcome.

For successful realization of experiments it is necessary to ensure the efficient excitation of SPPs. Because the dispersion relation of SPPs propagating along a smooth planar interface, ω_{SPP} (k), does not intersect the ω (k) light curve in the corresponding dielectric media,[1−3] the SPP excitation has to be provided by an interruption of surfaces smoothness, for example, via fabrication of one or more grooves or slits. Surface plasmon polaritons propagating toward each other from several grooves along the metal−dielectric interface provide a near-field interference pattern.

All mapping experiments have been carried out using a scanning near-field optical microscope, SNOM (NtegraSolaris NT-MDT), in the collection mode (Figure 1a). The electromagnetic near-field forming a pattern was coupled to a photomultiplier by an optical fiber with a 100 nm wide aperture in a metal-coated tip. The fiber tip was glued to a tuning fork possessing a resonant frequency of approximately 190 kHz and providing horizontal tip oscillations above the surface. The sample−tip distance was held constant (∼10 nm) by a feedback mechanism, similarly to the common noncontact AFM mode. The excitation laser beam (wavelength 633 nm, output power 15 mW) was guided by a multimode optical fiber into an inverted optical microscope and focused on a sample structure by an objective lens (Olympus, 20×, NA = 0.7) at the normal incidence. The laser spot was defocused in order to achieve more homogeneous illumination over the chosen area. The polarization direction of the incident light was set by a linear polarizer placed in front of the objective of the inverted microscope. The position of the sample with respect to the laser spot was adjusted by a sample holder equipped with a micromanipulator.

The structures were patterned by a focused ion beam (30 keV Ga^+) in a dual beam system (FIB - Tescan Lyra) into a 200 nm thick Au thin film (Figure 1b) deposited by Ar^+ ion-beam sputtering.[26] The patterns consisted of pairs of mutually tilted 150 nm wide slits (Figure 1c−e) or of four 4 μm-long slits arranged into a square (see Figure 1d). Both configurations of slits provided optimum conditions for measuring the SPP interference. The gold was chosen as a suitable plasmonic material because of its optical properties.[27] The higher thickness of the golden film was preferred in order to eliminate light transmission through it and to ensure that the SPPs generated at both interfaces do not interfere. To be able to find the correct wavelength and propagation length of SPPs (λ_{SPP} = 603 nm, L_{SPP} = 5.8 μm), the optical properties of gold [$\varepsilon(\lambda_0$ = 633 nm) = −10.6 + 1.7i] were determined by ellipsometry.[2]

The examples of measured electromagnetic near-field intensity on two slits tilted by 10° are shown in Figure 2a,b. A stripelike intensity pattern is observed using SNOM. These stripes can be explained in terms of the interference of near-field plane waves similarly as in case of the parallel-slit configuration.[23] The difference between maxima and minima of interference pattern intensity progressively changes with the polarization direction of incoming light; the maximum intensity

dx.doi.org/10.1021/nl400644r | Nano Lett. 2013, 13, 2558−2563

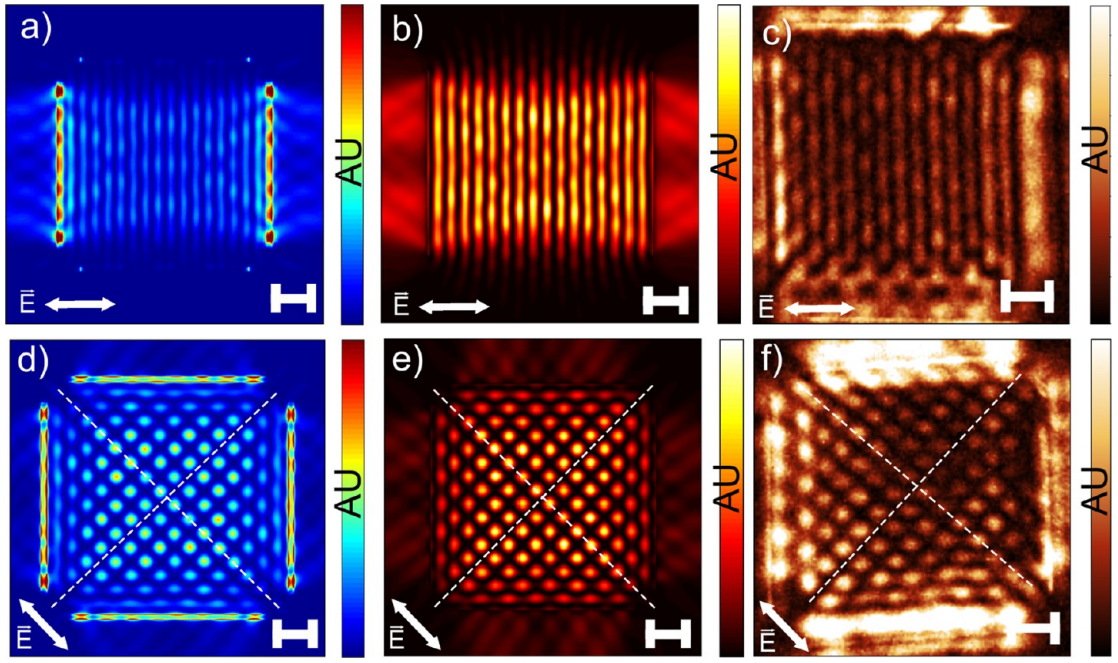

Figure 3. Numerical simulation (a), analytical calculation (b), and experimental SNOM image (c) of the near-field interference pattern established over the squarelike structure being illuminated homogeneously by the laser beam polarized in the direction perpendicular to two opposite slits (indicated by the horizontal white double arrow). Numerical simulation (d), analytical calculation (e), and experimental SNOM image (f) of the near-field interference pattern distributed over the squarelike structure illuminated homogeneously by the laser beam with polarization oriented in the diagonal direction (see the double arrow). In all the figures, the interference patterns formed by electric fields $|\mathbf{E}|^2$ are shown. The scale bars are 1 μm long.

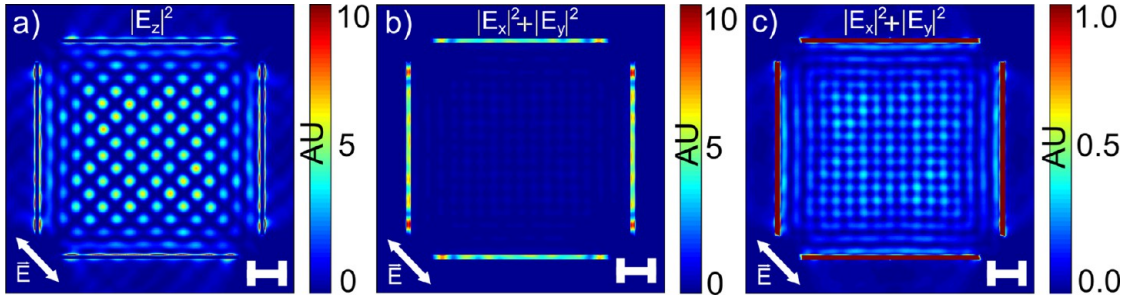

Figure 4. Simulated interference patterns formed on a homogeneously illuminated square-arranged structure by the out-of-plane (a) and in-plane components of the electric field (b,c). In (b) the same and in (c) the different z-scale range from that one in (a) is used.

modulation is achieved for the polarization direction perpendicular to the axis of the tilt angle. Moreover, the experimental results on the structures with the distinct tilt angle show an increasing trend of the mutual distance between the neighboring intensity maxima λ_m (modulation period) with the tilt angle. This trend can be modeled by two interfering plane waves propagating against each other under a mutual angle α, which gives the expression

$$\lambda_m = \frac{\lambda_{SPP}}{\sqrt{2 + 2\cos\alpha}} \quad (1)$$

The calculated results match with the experimental data (Figure 2c) if the wavelength 603 nm of the SPP on the gold−air interface is used. The uncertainty of the measured data with the mutual tilt angle is caused by the slit finite length.

To efficiently control the interference pattern via the polarization of incident light the square-arranged structures were prepared. In these structures, a transition between the stripelike and the dotlike interference patterns can be achieved.[24] In Figure 3c,f, the experimental results of both interference patterns on the homogeneously illuminated structure for appropriate directions of incident light polarization are shown. In case of the stripelike pattern, their period $\lambda_m \approx 300$ nm corresponds to the interference of two SPPs excited on the opposite slits by the light polarized perpendicularly to them (see eq 1 and Figure 2c). For the polarization in the direction of the square diagonal, the dotlike interference pattern is formed by regularly spaced spots (Figure 3f). Note that the interference pattern in Figure 3d−f exhibits a 2-fold symmetry that can be explained by the 180° initial phase-difference of SPPs propagating from separate pairs of neighboring slits. The phase shift is caused by the incident light polarization direction.[28]

To explain the experimental results on the square-shaped structures, 3D finite-difference time-domain (FDTD) simulations have been performed by Lumerical FDTD Solutions 7.5.5. The resulting near-field distribution $|\mathbf{E}|^2$ at the height of 10 nm above the surface is shown in Figure 3a,d. The simulated and experimental results are in a good qualitative agreement. It

dx.doi.org/10.1021/nl400644r | Nano Lett. 2013, 13, 2558−2563

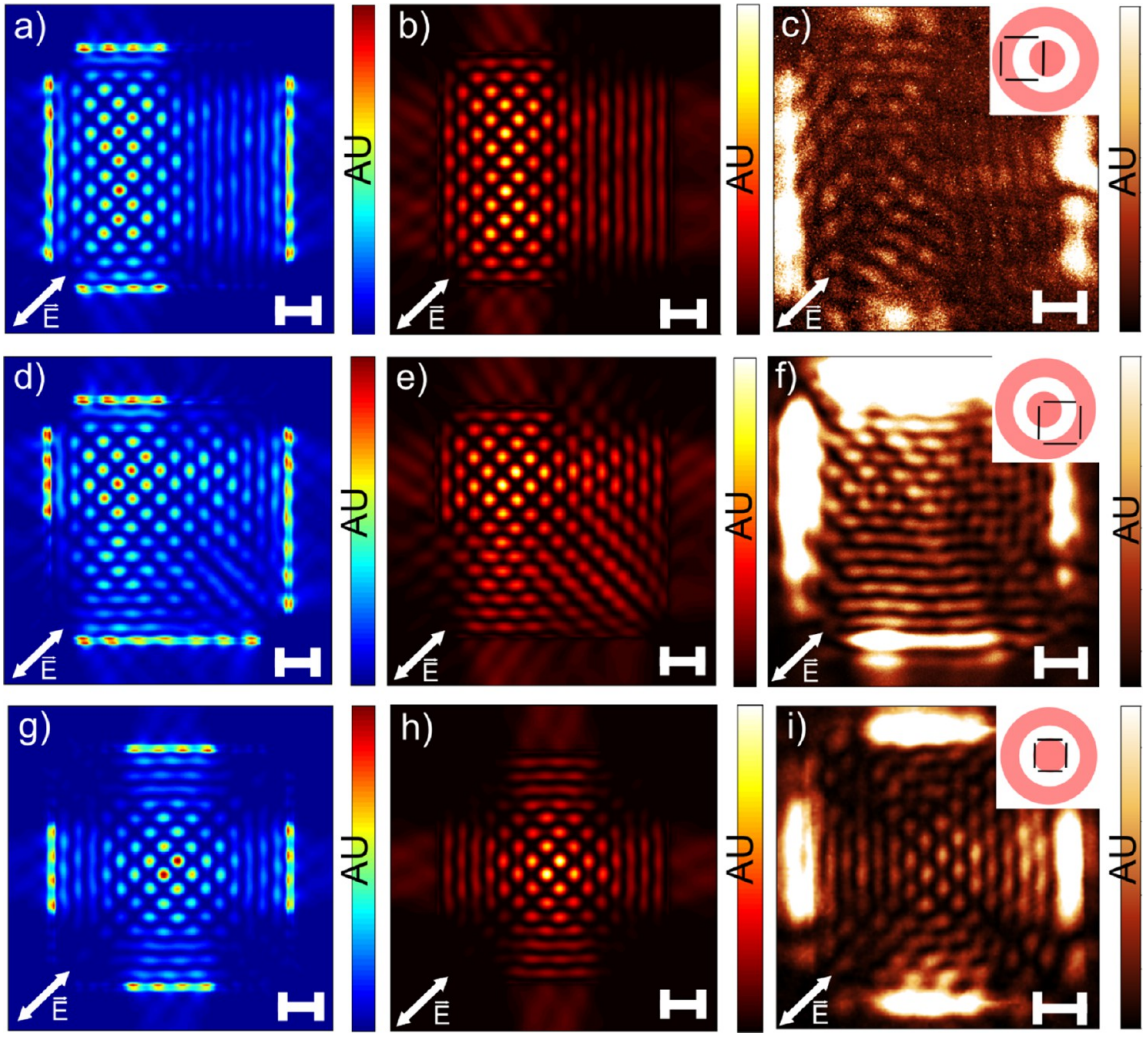

Figure 5. FDTD simulations (a,d,g), analytical calculations (b,e,h) and SNOM measurements of near-field interference patterns (c,f,i) detected on the square-arranged structure. The samples were illuminated by the incident laser beam polarized in the direction of the square diagonal. The way of illumination of slits is schematically depicted in the insets. The scale bars are 1 μm long.

shows that the distortion of the near field due to the probing tip is not significant. Figure 4 depicts the map of simulated square of modulus of the out-of-plane ($|E_z|^2$) and in-plane ($|E_x|^2 + |E_y|^2$) electric field components for the incident light polarization set in the direction of the square diagonal. By comparison of the magnitudes of in-plane and out-of-plane components it is clear that the z-component plays a primary role in the formation of the resultant interference pattern (note different scales in Figure 4).[29] Hence, in the analytical model presented below, only the interference of the z-component of the electric field is considered.

The considerable advantage of the analytical method used in our study is of a reasonably shorter computation time compared to the numerical simulation. In this analytical approach, every slit is represented by a series of point sources. The z-component of the electric field radiated by each point source along the plane was assumed to have the cosine angular distribution and to decrease with the distance by $1/\sqrt{r}$ (energy conservation).[29−31] The rigorous solution can be derived from the Green function of the 2D Helmholtz equation and the Rayleigh−Sommerfeld formalism.[32,33] Moreover, the finite propagation length is taken into account by introducing an exponential decay term. The radiation of a point source located at **a** is then approximately given by the expression

$$E_z(\mathbf{r}, t) \sim E_0(\mathbf{p}\cdot\mathbf{n})(\mathbf{n}\cdot\mathbf{e}_a)\frac{\cos(k_{SPP}r_a - \omega t)}{\sqrt{r_a}} \exp\left(-\frac{r_a}{2L_{SPP}}\right)$$

where E_0 and **p** are the electric field amplitude and the polarization direction of the illuminating light, respectively. Furthermore, $r_a = |\mathbf{r}_a| = |\mathbf{r} - \mathbf{a}|$ is the magnitude of a separation vector with $\mathbf{e}_a = \mathbf{r}_a/r_a$ being its unit vector. With **n** representing the normal vector to the slit (i.e., the direction of the maximum dipole radiation), terms $\mathbf{p}\cdot\mathbf{n}$ and $\mathbf{n}\cdot\mathbf{e}_a$ describe the role of the polarization on the efficiency of SPP excitation and the cosine angular distribution of the radiation, respectively. The constants k_{SPP} and L_{SPP} are the propagation constant and the propagation length of SPPs, respectively. The resulting interference patterns (corresponding to the time average value of $|E_z|^2$) are depicted in Figure 3b,e.

The detected SNOM signal is formed by complex light scattering processes between the tip and the sample, mixing different field components.[34,35] Thus, the electromagnetic field which couples to the probe cannot be simply connected to a specific component of the unperturbed electromagnetic field

dx.doi.org/10.1021/nl400644r | Nano Lett. 2013, 13, 2558−2563

distribution. However, as the E_z component in the interference patterns is 10 times larger compared to the in-plane components, it is reasonable to suppose that it represents the major part of the probe signal.

The electromagnetic near-field interference pattern on the square-arranged slits can be further modified. We demonstrate the possibility to handle the interference pattern by inhomogeneous illumination of the excitation slits. This can be achieved by a proper setup of the laser spot, that is, by adjusting the relative position of the spot with respect to the sample structure and setting the desired spot diffraction pattern (diffraction rings) by a specific focus. This approach is demonstrated by three examples. First, the horizontal slits are only half-illuminated. Second, the combined case when one pair of vertical and horizontal lines is only half-illuminated. Third, only the central parts of the slits are illuminated. The SNOM images of all corresponding interference patterns together with a schematic description of slit illumination (insets) are depicted in Figure 5c,f,i. In the first case, the near-field interference pattern consists of two parts (Figure 5c). The left part is similar to the interference pattern of the homogeneously illuminated square and is formed by regularly arranged spots. The rest of the pattern is dominated by a stripelike structure similar to Figurs 3a−c. The second case gives the near-field distribution that consists of three differently established interference patterns. Two of them form mutually perpendicular, periodically striped patterns; the residual area is filled by the spots. In the last case, there is again a combination of spots and a striped interference pattern. Theoretical calculations based on the Huygens−Fresnel principle and numerical simulations (FDTD) have been performed again to compare their results with the experimental data. In the analytical approach the amplitude of the secondary wave was considered as proportional to the electric field amplitude of illuminating light. By this approach it is possible to simulate SPP intensity distribution excited by any distribution of illumination light.

In conclusion, we have studied the interference of SPPs propagating along the metal−dielectric interface using the collective mode of SNOM. To carry out the experiments, we have fabricated metallic structures consisting of slits milled by FIB. The analytical model and FDTD numerical simulations have been utilized to support the experimental results and to predict the interference pattern shape. We have succeeded in monitoring the interference patterns and in modifying them both by variation of the angle between the slits (double-slit arrangement) and, for the fixed four-slit geometry, by combination of laser beam polarization and inhomogeneous illumination of the slits. We have shown that the performed measurements are in a good agreement with both the analytical and numerical models. Hence, the results of this work demonstrate the ability of the method to spatially control the near-field energy distribution. This can be utilized in nanolithography, trapping and selective growth of nanoparticles, and other fields of nanotechnology and nanoscience.

■ ASSOCIATED CONTENT

Supporting Information

Distribution of the magnetic field in a SPP interference pattern. This material is available free of charge via the Internet at http://pubs.acs.org.

■ AUTHOR INFORMATION

Corresponding Author

*E-mail: sikola@fme.vutbr.cz.

Notes

The authors declare no competing financial interest.

■ ACKNOWLEDGMENTS

This work was supported by the project GACR (P102/12/1881), European Regional Development Fund (CEITEC-CZ.1.05/1.1.00/02.0068), Grant of the Technology Agency of the Czech Republic (TACR) No. TE01020233, the EU seventh Framework Programme (Contract No. 286154 - SYLICA and 280566 - UnivSEM) and by the project GAVUT FSI-S-11-24, -J-12-30.

■ REFERENCES

(1) Novotny, L.; Hecht, B. *Principles of Nano-Optics*; Cambridge University Press: New York, 2006.

(2) Maier, S. A. *Plasmonics: Fundamentals and applications*, 1st ed.; Springer: New York, 2007.

(3) Raether, H. R. *Surface Plasmons on Smooth and Rough Surfaces and on Gratings*; Springer: New York, 1988.

(4) Fan, P.; Colombo, C.; Huang, K. C. Y.; Krogstrup, P.; Nygard, J.; Morral, A. F.; Brongersma, M. L. *Nano Lett.* **2012**, *12*, 4943−4947.

(5) Wei, H.; Li, Z.; Tian, X.; Wang, Z.; Cong, F.; Liu, N.; Zhang, S.; Nordlander, P.; Halas, N. J.; Xu, H. *Nano Lett.* **2011**, *11*, 471−475.

(6) Neutens, P.; van Dorpe, P.; de Vlaminck, I.; Lagae, L.; Borghs, G. *Nat. Photonics* **2009**, *3*, 283−286.

(7) Fan, P.; Chettiar, U. K.; Cao, L.; Afshinmanesh, F.; Engheta, N.; Brongersma, M. L. *Nat. Photonics* **2012**, *6*, 380−385.

(8) Feng, J.; Siu, V. C.; Roelke, A.; Mehta, V.; Rhieu, S. Y.; Palmore, G. T. R.; Pacifici, D. *Nano Lett.* **2012**, *12*, 602−609.

(9) Gao, Y.; Gan, Q.; Xin, Z.; Cheng, X.; Bartoli, F. J. *ACS Nano* **2011**, *12*, 9836−9844.

(10) Atwater, H. A.; Polman, A. *Nat. Mater.* **2010**, *9*, 205−213.

(11) Gopinath, A.; Boriskina, S. V.; Premasiri, W. R.; Ziegler, L.; Reinhard, B. M.; Negro, L. D. *Nano Lett.* **2009**, *9*, 3922−3929.

(12) Nie, S.; Emory, S. R. *Science* **1997**, *275*, 1102−1106.

(13) Yin, Y.; Li, T.; Xu, P.; Jin, H.; Zhu, S. *Appl. Phys. Lett.* **2011**, *98*, 093105.

(14) Wang, J.-Q.; Liang, H.-M.; Shi, S.; Du, J.-L. *Chin. Phys. Lett.* **2009**, *26*, 084208.

(15) Chen, Y.-F.; Serey, X.; Sarkar, R.; Chen, P.; Erickson, D. *Nano Lett.* **2012**, *12*, 1633−1637.

(16) Renaut, C.; Dellinger, J.; Cluzel, B.; Honegger, T.; Peyrade, D.; Picard, E.; de Fornel, F.; Hadji, E. *Appl. Phys. Lett.* **2012**, *100*, 101103.

(17) Liu, Z.; Steele, J. M.; Srituravanich, W.; Pikus, Y.; Sun, Ch.; Zhang, X. *Nano Lett.* **2005**, *5*, 1726−1729.

(18) Yin, L.; Vlasko-Vlasov, V. K.; Pearson, J.; Hillerm, J. M.; Hua, J.; Welp, U.; Brown, D. E.; Kimball, C. W. *Nano Lett.* **2005**, *5*, 1399−1402.

(19) Steele, J. M.; Liu, Z.; Wang, Y.; Zhang, X. *Opt. Express* **2006**, *14*, 5664−5670.

(20) Fang, Z.; Peng, Q.; Song, W.; Hao, F.; Wang, J.; Nordlander, P.; Zhu, X. *Nano Lett.* **2011**, *11*, 893−897.

(21) Drezet, A.; Stepanov, A. L.; Ditlbacher, H.; Hohenau, A.; Steinberge,r, B.; Aussenegg, F. R.; Leitner, A.; Krenn, J. R. *Appl. Phys. Lett.* **2005**, *86*, 074104.

(22) Zia, R.; Brongersma, M. L. *Nat. Nanotechnol.* **2007**, *2*, 426−429.

(23) Aigouy, L.; Lalanne, P.; Hugonin, J. P.; Julié, G.; Mathet, V.; Mortier, M. *Phys. Rev. Lett.* **2007**, *98*, 153902.

(24) Wang, Q.; Bu, J.; Yuan, X.-C. *Opt. Express* **2010**, *18*, 2662−2667.

(25) Gjonaj, B.; Aulbach, J.; Johnson, P. J.; Mosk, A. P.; Kuipers, L.; Lagendijk, A. *Nat. Photonics* **2011**, *5*, 360−363.

(26) Urbánek, M.; Uhlíř, V.; Bábor, P.; Kolíbalová, E.; Hrnčíř, T.; Spousta, J.; Šikola, T. *Nanotechnology* **2010**, *21*, 145304−145310.

(27) Park, J. H.; Nagpal, P.; Oh, S.-H.; Norris, D. J. *Appl. Phys. Lett.* **2012**, *100*, 081105.
(28) Ung, B.; Sheng, Y. *Proc. SPIE* **2007**, *6832*, 68320E.
(29) Ginzburg, P.; Hirshberg, E.; Orenstein, M. *J. Opt. A: Pure Appl. Opt.* **2009**, *11*, 114024.
(30) Steele, J. M.; Liu, Z.; Wang, Y.; Zhang, X. *Opt. Express* **2006**, *14*, 5664−5670.
(31) Hecht, B.; Bielefeldt, H.; Novotny, L.; Inouye, Y.; Pohl, D. W. *Phys. Rev. Lett.* **1996**, *77*, 1889−1892.
(32) Sommerfeld, A. *Optics*; Academic Press: New York, 1954.
(33) Zayats, A. V.; Smolyaninov, I. I.; Maradudin, A. A. *Phys. Rep.* **2005**, *408*, 131−314.
(34) Novotny, L.; Pohl, D. W.; Hecht, B. *Opt. Lett.* **1995**, *20*, 970−972.
(35) Martin, O. J. *J. Microsc.* **1999**, *194*, 235−239.

dx.doi.org/10.1021/nl400644r | *Nano Lett.* 2013, 13, 2558−2563